Journal of MATERIALS RESEARCH

Invited Paper
DOI:10.1557/s43578-021-00114-8

MULTISCALE MATERIALS MODELING OF INTERFACE-MEDIATED THERMOMECHANICAL BEHAVIOR

Thermal stable hierarchical 3D nanolayered Zr-2.5Nb

Xiao-Wei Zou[1], Jie-Wen Zhang[1], Wei-Zhong Han[1,a)]

[1] Center for Advancing Materials Performance From the Nanoscale, State Key Laboratory for Mechanical Behavior of Materials, Xi'an Jiaotong University, Xi'an 710049, People's Republic of China

[a)] Address all correspondence to this author. e-mail: wzhanxjtu@mail.xjtu.edu.cn

Received: 20 November 2020; accepted: 21 January 2021; published online: 4 February 2021

Hierarchical 3D nanolayered Zr-2.5Nb has high strength, strain hardening and ductility because of the 3D α/β-Zr networks, which is a promising structural material for nuclear reactor. However, excellent thermal stability is of great importance for materials service in nuclear reactor. Here, we study thermal stability of the hierarchical 3D nanolayered Zr-2.5Nb. After 1 h annealing at various temperatures below 700 °C, α-Zr layer thickness only has a slightly increase. The hardness, yield strength and uniform elongation of the sample remain unchanged. Interface orientation relationship and layer morphology keep stable after annealing, indicating high thermal stability. The duplex phase structures coarsen quickly after annealing at 1000 °C. An obvious increase in hardness and yield strength was observed when sample annealed at 300 °C, which relates to the precipitation of ω_{iso} phase in β-Zr. Controlling the number of ω_{iso} phase is likely a strategy to further enhance the strength and ductility of the alloy.

Introduction

Zr-2.5Nb alloys have drawn attention because of a combination of low thermal neutron scattering cross-section, high strength and good corrosion resistance [1, 2]. As a result, Zr-2.5Nb alloys are widely used in the nuclear reactor as pressure vessels and fuel claddings [3–5]. Because of ever-increasing demands on structural materials for new generation nuclear reactors, vast improvements in strength, toughness, radiation tolerance, corrosion resistance are critically needed [1].

Traditional methods used to improve the strength include solid solution strengthening [6, 7], dispersion strengthening [7, 8], strain hardening [9] and grain refinement [10, 11] etc. The common feature in these methods is to introduce various defects and boundaries to obstruct dislocation motion [11, 12]. The strength of metals can be improved effectively using these methods, however, a notable decrease in ductility and toughness always occurs [11]. Several reports show that the strength and ductility of metallic materials can be simultaneously increased via microstructural refinement down to nanoscale [13, 14]. In our previous work, a novel hierarchical 3D nanolayered microstructure has been developed in Zr-2.5Nb alloy via dynamic thermal–mechanical phase transformation (DTMPT) method [1]. It is composed of coarse grains filled with microscale colonies, each of which are nanolaminated with numerous α/β-Zr phase lamellae. The α-Zr phase has hexagonal close packed (HCP) crystal structure with an average layer thickness of 222 ± 94 nm, while the β-Zr phase is of body centered cubic (BCC) structure with average layer thickness of 10 to 20 nm [1]. The α/β-Zr duplex interface has a classical Burgers orientation relationship $[0001]_\alpha//[011]_\beta$ and $(\bar{1}\,\bar{1}\,20)_\alpha//(111)_\beta$, which is not atomically flat but comprised of a series of facets [1]. Moreover, the angle between α/β-Zr duplex interface and the prismatic plane $(\bar{1}\,100)$ of α-Zr phase is ~ 10° [1]. Due to strong obstruction of α/β-Zr interface on dislocations, the hierarchical 3D nanolayered biphase Zr alloy exhibits high yield strength, strain hardening and toughness [1], making it a promising structural material for nuclear reactors. The thermal stability of the alloy is of concern because of the cladding tubes in nuclear reactor service in the temperature range of 300 °C to 500 °C [15]. However, in general, poor thermal stability is one of the inherent drawbacks in nanostructured metals owing to the amount of interfaces [16].

In general, grain growth occurs in nanocrystalline Cu even at room temperature [17]. Similarly, the grain size of ultrafine grained Cu can be enlarged by an order of magnitude even after annealing at 200 °C [18]. The driving force for grain growth relate to the size of grain and the boundary energy according to the Gibbs–Thomson equation [19], $P = \frac{4\gamma}{d}$, where P is the

driving force for grain growth, γ is the interface energy and d is the grain size. The driving force of grain growth increases with the increasing of boundary energy and the decreasing of grain size, which are origins for poor thermal stability of nanostructured metals [17, 20]. Moreover, by diffusive mass transport at elevated temperature, polycrystalline multilayers become thermally unstable, because grooves develop at the triple-point junctions, where a grain boundary intersects the bimetal interface [21]. As a result, the stability of polycrystalline multilayers is of question due to thermal grooving at columnar grain boundaries, which leads to layer pinch-off at elevated temperatures [21]. What's more, the mobility of the boundary and the interface structures also affect the grain or phase growth by affecting the migration rate of the interface [20]. Because of the low-energy bimetal interface, the hardness of nanolaminated Cu/Nb composites with a thickness of 10 nm has a slightly decrease from 4.13 ± 0.4 GPa to 4.07 ± 0.2 GPa after annealing at 500 °C for 1 h and the sample maintains layered morphology with flat and sharp interfaces. In addition, the layer thicknesses increase by a small amount and their distribution broadens slightly, indicating high thermal stability [22]. Nanotwined Cu also exhibits good thermal stability owing to a high fraction of low-energy coherent twin boundaries. For instance, the average twin lamellae thickness has a modest increase from 4 to 16 nm as well as a broader distribution even annealed at 800 °C for 1 h, and the hardness of the as-received nanotwinned Cu films gradually decreases from ~ 3.5 GPa to approximately 2.2 GPa after annealing at 800 °C, which is much slower than the hardness decrease of ultra-fined grained and nanocrystalline Cu after annealing at 400 °C [18]. Therefore, high thermal stability could achieve in interface engineered metals through proper design [22, 23].

Despite the high mechanical strength and excellent toughness of the hierarchical 3D nanolayered Zr-2.5Nb alloy, their thermal stability at elevated temperatures remains to be evaluated. The faceted interface structure in Zr-2.5Nb will likely induce thermal instability [1]. In this study, we investigated the thermal stability of the hierarchical 3D nanolayered Zr-2.5Nb alloy through annealing experiment, microstructural characterization and mechanical test. We found that the hierarchical 3D nanolayered Zr-2.5Nb is thermally stable till 700 °C.

Results and discussion

Microstructural evolution

Scanning electron microscope (SEM) images of the as-received hierarchical 3D nanolayered Zr-2.5Nb and annealed samples are shown in Fig. 1. For annealing in the temperature range of 200 °C—500 °C, the layered morphology remains unchanged. The α/β-Zr lamellar interface keeps flat and sharp, and α-Zr lamellae do not coarsen. The duplex interface structure changes slightly after annealing at 600 °C; α-Zr phase lamellae become thicker and the duplex interfaces become diffuse, as shown in Fig. 1f. This indicates that only a small amount of phase transition from α-Zr phase to β-Zr phase occurs. Part of transformed β-Zr phase remained, which makes the duplex boundaries fuzzy. With further increasing the annealing temperature to 700 °C, α-Zr phase to β-Zr phase transformation becomes more obvious; The original β-Zr lamellae still existed and the newly precipitated β-Zr phases are partially retained after furnace cooling. Therefore, the β-Zr lamellae become discontinuous, while the morphology of α-Zr lamellae do not change significantly, as shown in Fig. 1g. Phase transition from α-Zr to β-Zr occurs after annealing at 800 °C, thus more β-Zr phase remained after cooling, as shown in Fig. 1h. Therefore, discontinuous β-Zr lamellae occupy a large fraction (Fig. 1h) after annealing at 800 °C. After annealing at 1000 °C for 1 h, the layered microstructures coarsen obviously. As shown in Fig. 1i, α-Zr lamellar thickness increased significantly. According to the binary phase diagram, when the annealing temperature reaches 1000 °C, Zr-2.5Nb alloy enters β-Zr phase zone and all α-Zr phase convert into β-Zr phase. Because no plastic deformation treatment is carried out before β-Zr to α-Zr phase transformation during furnace cooling, the number of α-Zr phase nucleation site is scarce. Thus, most of α-Zr phase nucleated from grain boundaries during furnace cooling, which resulting in coarsening of α-Zr lamellae. The density of α/β duplex interfaces decreases, as a result, the hierarchical 3D nanolayered structure is destroyed and transforms into a 2D coarse-layered structure.

The distribution of the lamellar thickness for the as-received and the annealed hierarchical 3D nanolayered Zr-2.5Nb are shown in Fig. 2. The average thickness of the α-Zr lamellae do not increase significantly as the temperature increases for annealing below 700 °C. The average thickness of α-Zr lamellae has slightly increased from 251 ± 122 nm for as-received specimen to 300 ± 129 nm for annealing at 600 °C for 1 h. With further increasing the annealing temperature to 700 °C, the average thickness of α-Zr lamellae increases modestly to 385 ± 171 nm as well as a broader distribution. Moreover, the average thickness of α-Zr lamellae increases rapidly to 611 ± 231 nm after annealing at 800 °C for 1 h. Notably, the thickness of α-Zr lamellae increases to 890 ± 576 nm after annealing at 1000 °C for 1 h, which is even higher than a previous 2D coarse-layered Zr-2.5Nb (589 ± 227 nm) [1]. The previous 2D coarse-layered alloy is prepared via annealing at 1000 °C for 15 min followed by air cooling to room temperature [1], while the 1000 °C annealing of the hierarchical 3D nanolayered Zr-2.5Nb lasts for 1 h. The increased annealing time at β phase zone leads to larger β-Zr grain size or reduced grain boundary density, as a result, there are low density of α-Zr nucleation sites. Moreover, the furnace cooling of 1000 °C annealed hierarchical 3D nanolayered Zr-2.5Nb make the β-Zr to α-Zr phase transformation slower, and the growth time of α-Zr lamellae longer. Hence higher average

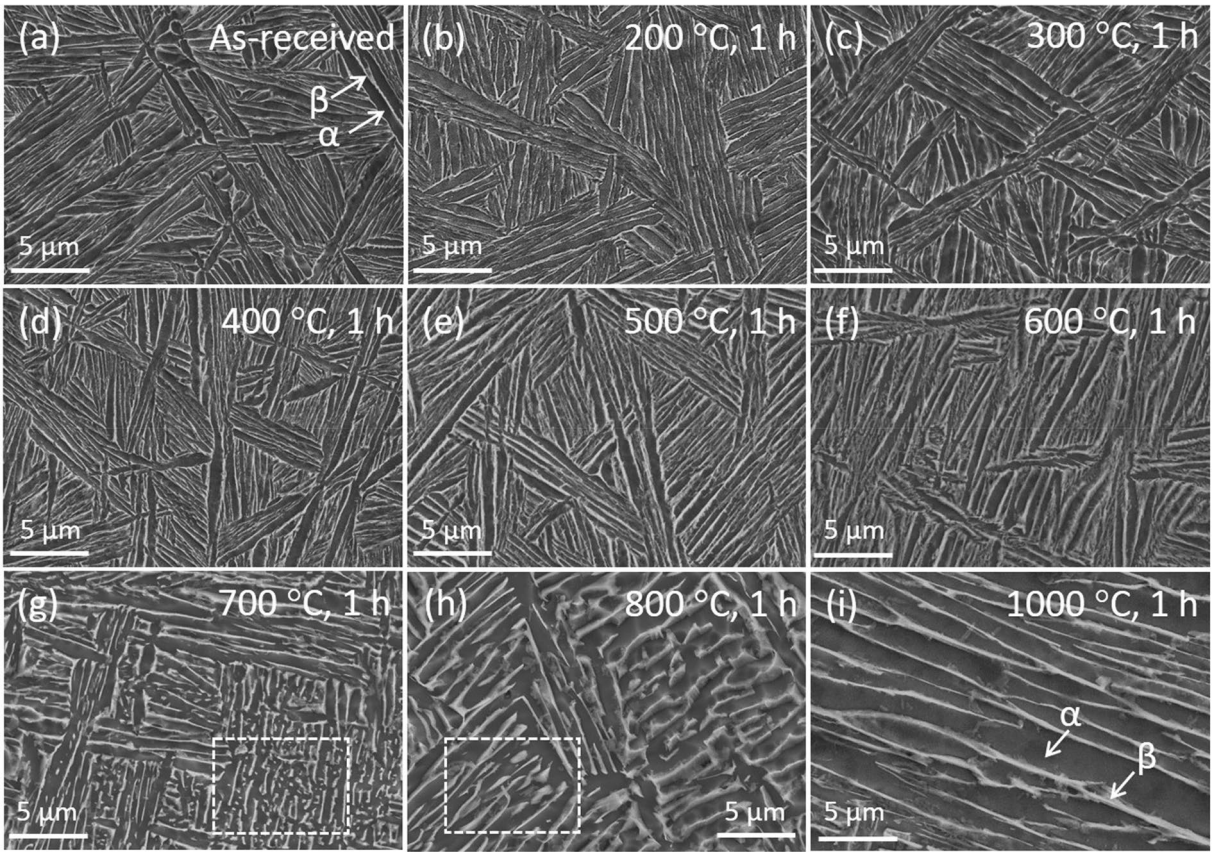

Figure 1: SEM images of hierarchical 3D nanolayered Zr-2.5Nb: (a) As-received sample and specimens annealed at (b) 200 °C, (c) 300 °C, (d) 400 °C, (e) 500 °C, (f) 600 °C, (g) 700 °C, (h) 800 °C and (i) 1000 °C for 1 h.

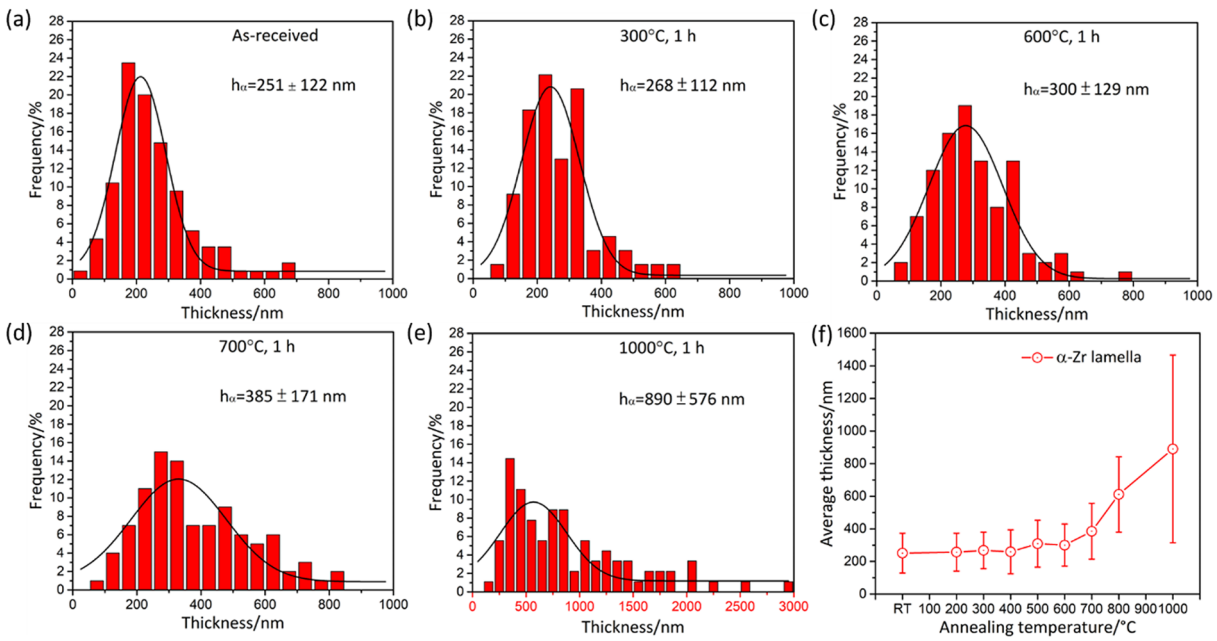

Figure 2: Statistical distributions of α-Zr layer thickness in (a) As-received sample and specimens annealed at (b) 300 °C, (c) 600 °C, (d) 700 °C, (e) 1000 °C for 1 h. (f) Variation of α-Zr layer thickness with annealing temperature.

layer thickness of α-Zr lamellae after annealed at 1000 °C than that of previous 2D coarse layered alloy [1]. Furthermore, unlike traditional metallic multilayer with several nano-scale grain or grain boundaries inside a single layer, there is no groove forms at α/β-Zr interface, due to the lack of grain boundaries inside a single α-Zr or β-Zr layer, resulting in the unchanged α/β lamellar morphology [1]. The statistics of layer thickness show that a remarkable thermal stability of hierarchical 3D nanolayered Zr-2.5Nb below 700 °C. Even at temperatures close to the monotectoid reaction temperature of 610 °C [24], no significant coarsening of α-Zr lamellae was discerned according to SEM observations.

Figure 3 shows the XRD patterns of the as-received and the annealed specimens. Two types of diffraction peaks are identified in the as-received specimen, such as α-Zr and β-Zr phases, respectively. For annealing at 300 °C, a new diffraction peak for ω phase at 2θ of 59° can be detected, as highlighted in Fig. 3b. Two kinds of ω phase can be obtained either by rapidly quenching from the β-phase region (athermal ω phase, ω_{ath}) or product of thermally activated β-phase decomposition (isothermal ω phase, ω_{iso}) in Zr-2.5Nb alloy [11, 25–27]. Crystal structure of the ω phase is either hexagonal with space group of P6/mmm or trigonal with space group of P $\bar{3}$ m1, depending on the solute concentration [28]. The orientation relationship is $(111)_\beta$//$(0001)_\omega$ and $[1\ \bar{1}\ 0]_\beta$//$[1\ \bar{2}\ 10]_\omega$ for athermal and isothermal ω phase [29, 30]. The athermal β → ω transformation is displacive, diffusionless of the first-order, and thus the obtained ω phase has a composition very close to that of the β-Zr phase. The athermal ω phase are very fine (< 5 nm) and it is difficult to assign any well-developed geometrical shape for these particles which tend to align along $<111>_\beta$ [28, 29]. The thermally activated β → ω transformation is accompanied by solute redistribution. The solute lean regions of β-Zr phase are eventually transformed to the ω_{iso} phase [25, 30, 31]. The shapes of ω_{iso} phase have two types of morphologies, ellipsoidal and cubic [32]. According to these characteristics, the ω phase here is ω_{iso} phase which precipitated during the annealing process [11, 25–33]. Almost no diffraction peak of ω_{iso} phase was detected for annealing in the range of 400–1000 °C, which suggests the dissolution of ω phase take place with further increasing of the annealing temperature.

Lamellar structure evolution

Transmission electron microscope (TEM) images and the corresponding selected diffraction patterns of the as-received and the annealed specimens are shown in Fig. 4. The α-Zr lamellae and β-Zr lamellae stack alternately. According to the diffraction pattern in Fig. 4a, the α/β-Zr interface has a Burgers orientation relationship $[0001]_\alpha$//$[011]_\beta$ and $(\bar{1}\bar{1}\ 20)_\alpha$//$(1\ \bar{1}\ 1)_\beta$ for the as-received specimen. Moreover, part of β-Zr lamellae are not quite flat, but rather intermittent which is different from SEM observations in Fig. 1a. During air cooling process in DTMPT, different β-Zr lamellae touch or connect to each other, but a small amount of β-Zr phase transform to α-Zr phase occurs at the junctions is likely responsible for the intermittent β-Zr lamellae. There is some ω_{iso} phase precipitated from the solute lean regions of β-Zr phase according to the XRD characterization for specimen annealed at 300 °C for 1 h. In Fig. 4b, both α-Zr lamellae and β-Zr lamellae did not coarsen significantly. Meanwhile, no ω_{iso} precipitation can be observed in the nanoscale β-Zr lamellae likely due to weak diffraction signal

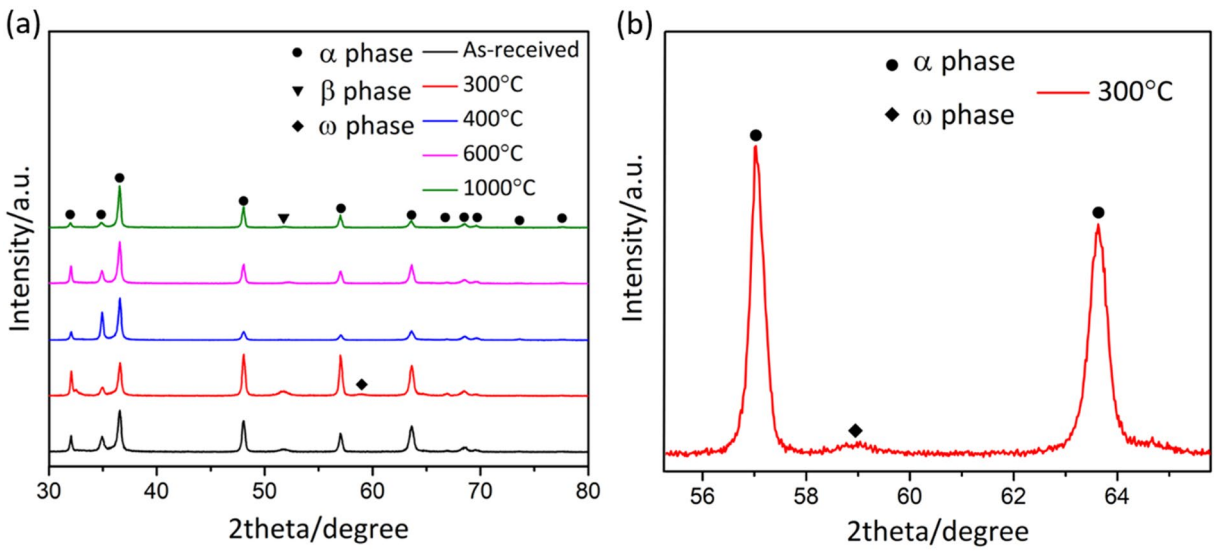

Figure 3: XRD patterns of hierarchical 3D nanolayered Zr-2.5Nb annealed at various temperatures for 1 h: (a) Full range of XRD patterns; (b) Enlarged XRD pattern for specimen annealed at 300 °C.

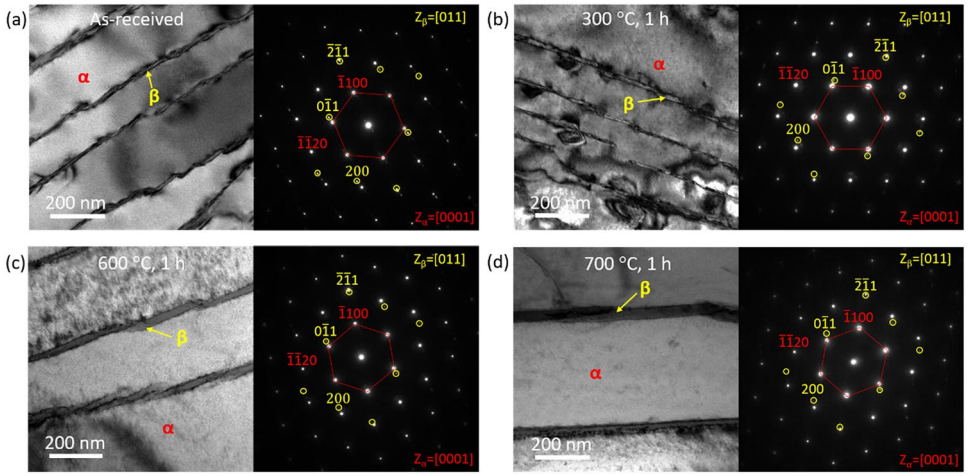

Figure 4: TEM micrographs and selected area diffraction pattern of (a) As-received sample and specimens annealed at (b) 300 °C, (c) 600 °C and (d) 700 °C for 1 h.

from ω_{iso} phase in a single layered β-Zr. Moreover, the amount of ω_{iso} phase is low and their size is too small to be detected in the nanoscale β-Zr lamellae.

As shown in Fig. 4c and d, after annealing at 600 °C and 700 °C, the thickness of α-Zr lamellae increased obviously and the coarsening of β-Zr lamellae indicated that α → β phase transformation has happened because part of transformed β-Zr phase retained during the subsequent cooling, which is consistent with the SEM observations. The morphology of β-Zr lamellae did not change significantly, which still join with different β-Zr lamellae. According to the diffraction pattern, the α/β-Zr phases still have the Burgers orientation relationship. The angle between the interface and the $(\bar{1}\ 100)$ plane of α-Zr phase is still around 10° after annealing, comparable to the as-received sample [1]. In addition, there is no grain boundary exist in either α-Zr or β-Zr lamellae because the internal orientation of each lamella is consistent, which is different from the nanolayered Cu/Nb films fabricated by magnetron sputtering [24] and accumulative rolling bonding [22], or duplex Zr-2.5Nb manufactured by hot-rolled deforming at α + β duplex zone [27]. As a result, no groove is observed in α/β-Zr lamellae, resulting in the thermal stability of α/β-Zr duplex lamellae. These observations indicate that the duplex microstructures are stable up to 700 °C, which show the hierarchical 3D nanolayered Zr-2.5Nb has good thermal stability in a wide temperature range.

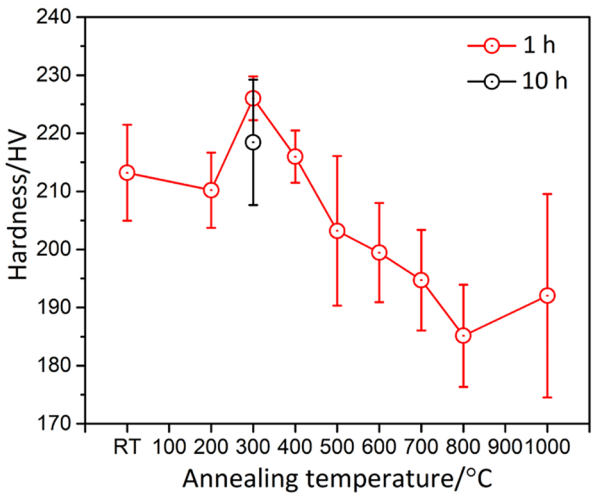

Figure 5: Hardness variation of hierarchical 3D nanolayered Zr-2.5Nb annealed at different conditions.

Mechanical properties

Figure 5 and Table 1 show the variation of micro-Vickers hardness of specimens annealed at different conditions. The micro-Vickers hardness firstly decreases from the original value of 213 HV to 210 HV after annealing at 200 °C, and then increases to the highest value of 226 HV at 300 °C. Finally, the hardness decreases to 192 HV after annealing at 1000 °C. Moreover, the hardness is slightly lower for annealing at 300 °C for 10 h (218 HV) than that of 1 h (226 HV). The decrease of hardness is related to the decrease of dislocation density in α-Zr lamellae. The precipitation of ω_{iso} particles are origin for the increase of hardness after annealing at 300 °C although the dislocation density maybe decreased after annealing. The volume fraction of the ω_{iso} phase forming in the β-Zr matrix is a function of the reaction time, it will increase first and then decrease which depends on the diffusion controlled partitioning of the solute between solute lean and solute rich β-Zr regions [8, 30]. Therefore, with further annealing, ω_{iso} phase dissolves continuously, which decreases the hardness of sample annealed at 300 °C for 10 h. For annealing at 1000 °C, α-Zr lamellae coarsen significantly, colonies disappear, and dislocation density decreases, all of these factors cause lower hardness. In addition, the microstructural

TABLE 1: Micro-Vickers hardness of hierarchical 3D nanolayered Zr-2.5Nb annealed at different conditions.

Temperature (°C)	RT	200	300		400	500	600	700	800	1000
Time (h)	–	1	1	10	1	1	1	1	1	1
Hardness/HV	213 ± 8	210 ± 7	226 ± 4	218 ± 11	216 ± 5	203 ± 13	200 ± 9	195 ± 9	185 ± 9	192 ± 18

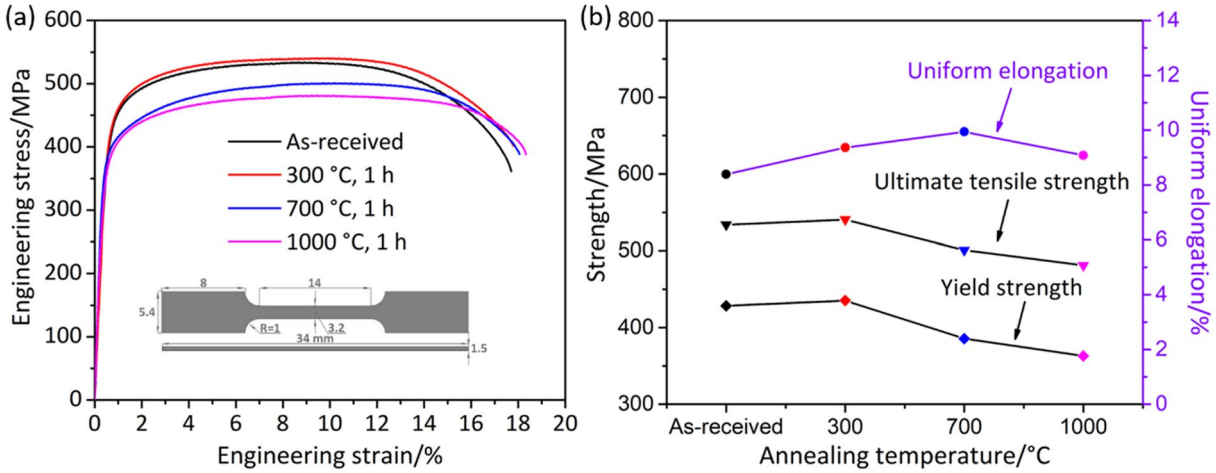

Figure 6: Tensile properties of hierarchical 3D nanolayered Zr-2.5Nb annealed at different temperatures (a) Engineering stress–strain curves; (b) Variation of strength and elongation with annealing temperature.

transformation from 3D to 2D due to the spatial interface rearrangement. The heterogeneous microstructures induce a larger error bar in hardness in Fig. 5.

Tensile engineering stress–strain curves of the as-received sample and specimens annealed at 300 °C, 700 °C and 1000 °C for 1 h are displayed in Fig. 6 and summarized in Table 2. After annealing at 300 °C for 1 h, the yield strength and the ultimate tensile strength increase slightly from 428 MPa and 533 MPa to 435 MPa and 540 MPa, respectively. The uniform elongation also increases from 8.39% to 9.36%. It means a small amount of ω_{iso} phase increases the strength and ductility simultaneously. Slip transmission of dislocations along $(10\bar{1}0)_\alpha$-$(0\bar{1}1)_\beta$ occur at the later stage of uniform deformation in the as-received nanolayered Zr-2.5Nb alloy [1], which means dislocations could cut through the β-Zr lamellae. In contrast, precipitation of ω_{iso} phase after annealing at 300 °C prevents dislocations cutting through the β-Zr lamellae, which strengthens the nanolayered duplex Zr-2.5Nb alloy and leads to the dislocations pile-up at interfaces. Therefore, precipitation of ω_{iso} phase enhances the strain hardening rate, yield strength and uniform elongation simultaneously. Moreover, the internal stress will reduce as dislocation density decreases. Thus, the specimen annealed at 300 °C for 1 h also has improved ductility. When the specimen is annealed at 700 °C for 1 h, the yield strength and ultimate tensile strength decrease to 385 MPa and 500 MPa, respectively. The uniform elongation evolution is inverse to the strength, which slightly increases to 9.94%, and comparable to the as-received specimen. With further increasing the annealing temperature to 1000 °C, the yield strength and tensile strength significantly decrease to 362 MPa and 481 MPa, respectively. The uniform elongation slightly increases to 9.08%. The coarsening of the α-Zr lamellae, resulting in the decrease of the α/β-Zr duplex interfaces, which makes the motion of dislocations easier. In addition, the disappearance of the 3D colonies as well as the decreasing of dislocation density lead to lower yield strength in these samples. In general, the strength of the annealed samples although decrease but less than 16% compared to the as-received specimens, displaying a good mechanical stability after high temperature annealing.

TABLE 2: Tensile properties of hierarchical 3D nanolayered Zr-2.5Nb alloy annealed at different temperatures.

Temperature (°C)	$\sigma_{0.2}$ (MPa)	σ_b (MPa)	δ_u (%)
As-received	428.34	533.69	8.39
300	435.28	540.45	9.36
700	385.53	500.89	9.94
1000	362.93	481.21	9.08

The fracture surface of the as-received and the annealed specimens are shown in Fig. 7. All samples display a typical ductile fracture mode. High density of dimples are produced. The ductile fracture consists of three distinct stages: micro-voids nucleation where the severe ductile deformation occurred in the first stage, micro-voids growth with the continuous action of the stress in the second stage, and then micro-voids coalesce into

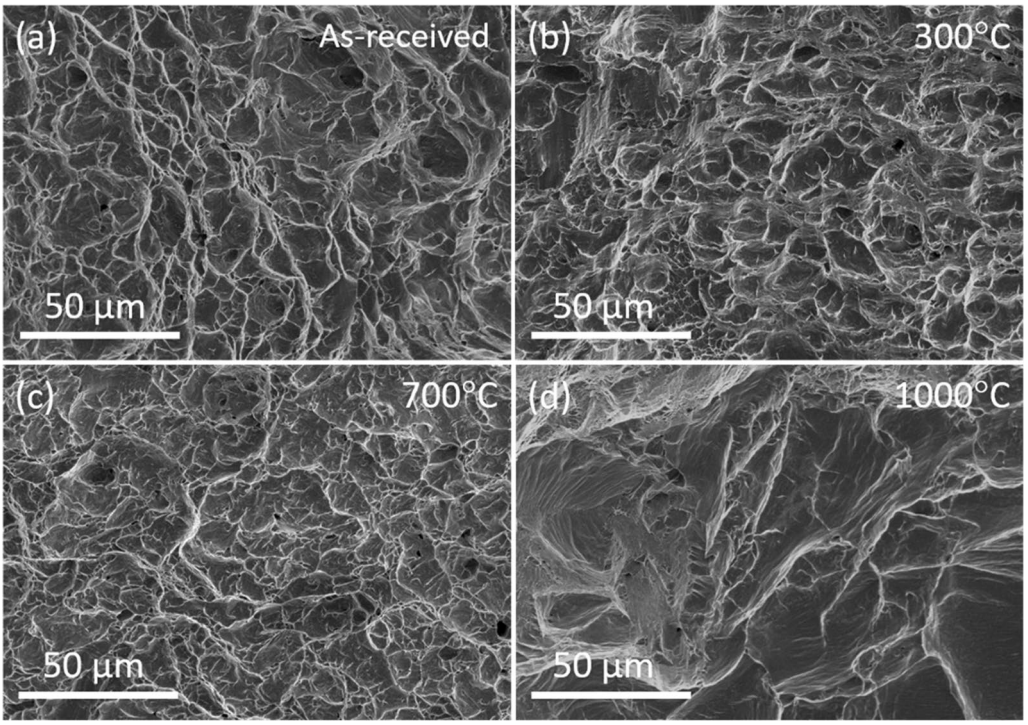

Figure 7: Tensile fracture morphology of hierarchical 3D nanolayered Zr-2.5Nb: (a) As-received sample; Specimen annealed at (b) 300 °C, (c) 700 °C and (d) 1000 °C for 1 h.

crack [34, 35]. According to Table 2, the ductility of the annealed specimens remain unchanged. Micro voids can preferentially nucleate at α/β-Zr duplex interface, and the morphology of dimples are related to colonies in each grain. As shown in Fig. 7a–c, the size and depth of dimples are same in the as-received sample and specimens annealed at 300 °C and 700 °C due to the unchanged size of colonies. However, the size and depth of dimples increase obviously in sample annealed at 1000 °C for 1 h as a result of significantly increased area of colonies. The variation in size of dimples reflect the hierarchical 3D microstructures remaining stable until 700 °C, and gradually transform into coarse 2D layered microstructures after annealing at 1000 °C.

Conclusions

In this paper, the microstructural stability and corresponding mechanical properties of the hierarchical 3D nanolayered Zr-2.5Nb alloy annealed at different conditions were investigated. Main findings are as following:

(1) Hierarchical 3D nanolayered Zr-2.5Nb has good thermal stability till 700 °C. Layered thickness and morphology remain unchanged. The α-Zr and β-Zr phases still maintain the classical Burgers orientation relationship below 700 °C.

(2) Once annealing temperature higher than 700 °C, the thickness of duplex lamellae increases significantly, and β-Zr lamellae become intermittent. The coarsening of layered structure leads to significant decrease of hardness and strength.

(3) A certain amount of ω_{iso} phase with a faint diffraction peak precipitated from the β-Zr lamellae when annealed at 300 °C for 1 h. Strength and ductility of sample are enhanced due to a small amount of ω_{iso} phase.

Experimental methods

Hierarchical 3D nanolayered Zr-2.5Nb alloy was fabricated using a DTMPT method [1]. Specimens for microstructural observations were annealed at 200 °C, 300 °C, 400 °C, 500 °C, 600 °C, 700 °C, 800 °C, 1000 °C for 1 h and 300 °C for 10 h using a tube furnace with a vacuum of 1.3×10^{-4} Pa. Microstructural characterization was performed using scanning electron microscope (SEM, Hitachi SU6600) and transmission electron microscope (TEM, FEG JEOL 2100F), respectively. Samples for SEM observation were first polished and then etched using a mixture of 10 vol.% hydrofluoric acid, 40 vol.% nitric acid and 50 vol.% distilled water. Thin foils for TEM observation were first ground to a thickness of approximately 50 μm and then further thinned by twin-jet polishing in a solution of 10 vol.% perchloric acid and 90 vol.% ethanol under an operation voltage of 25 V at − 40 °C. X-ray diffraction (XRD) profiles were

collected for each annealed specimen using a Bruker diffractometer with Cu Kα radiation. The diffraction profiles were obtained by varying 2θ from 30° to 80° with a step scan of 0.02° and the time spent collecting the data per step was 0.1 s. Micro-Vickers hardness was measured at room temperature under a load of 200 gf and holding for 10 s after the samples were polished. At least 10 valid spots were tested on each sample. Specimens for tensile tests were cut into dog-bone samples with size of 14 mm (length) × 3.2 mm (width) × 1.16 mm (thickness) by an electric spark cutting machine. Quasi-static tensile tests were performed at room temperature with a constant displacement rate of 0.84 mm/min, corresponding to an initial strain rate of 1×10^{-3}/s using an MTS tensile machine with an extensometer. More than 3 tests were repeated for each type of sample. The fracture surface morphologies of specimens were observed using SEM to characterize the fracture mode.

Acknowledgments

This work was supported by the National Natural Science Foundation of China (Grant Nos. 51922082, 51971170 and 51942104), the National Key Research and Development Program of China (2017YFB0702301), the 111 Project of China (Grant Number BP2018008) and the Innovation Project of Shaanxi Province (Grant Number 2017KTPT-12).

Data availability

Data related to this manuscript are available on reasonable request.

Compliance with ethical standards

Conflict of interest The authors declare there is no conflict of interest.

References

1. J.W. Zhang, I.J. Beyerlein, W.Z. Han, Hierarchical 3D nanolayered duplex-phase Zr with high strength, strain hardening, and ductility. Phys. Rev. Lett. **122**(25), 255501.1–255501.7 (2019).
2. J.W. Zhang, B. Leu, M.A. Kumar, M. Arul Kumar, I.J. Beyerlein, W.Z. Han, Twin hopping in nanolayered Zr-2.5Nb. Mater. Res. Lett. **8**(8), 307–313 (2020).
3. R.A. Holt, In-reactor deformation of cold-worked Zr–2.5Nb pressure tubes. J. Nucl. Mater. **372**, 182 (2008).
4. K. Holm, J.D. Embury, G.R. Purdy, The structure and properties of microduplex Zr-Nb alloys. Acta Metall. **25**, 1191 (1977)
5. N. Saibaba, Kumar Vaibhaw, S. Neogy, K.V. Mani Krishna, S.K. Jha, C. Phani Babu, S.V. Ramana Rao, D. Srivastava, G.K. Dey, Study of microstructure, texture and mechanical properties of Zr–2.5Nb alloy pressure tubes fabricated with different processing routes. J. Nucl. Mater. **440**, 319 (2013).
6. H. Somekawa, Y. Osawa, T. Mukai, Effect of solid-solution strengthening of fracture toughness in extruded Mg–Zn alloys. Scr. Mater. **55**, 593–596 (2006)
7. D.L. Douglass, The relative contributions of dispersion and solution strengthening in Zr–Sb–Nb alloys. J. Nucl. Mater. **9**, 252–260 (1963)
8. K.C. Antony, H.H. Klepfer, Dispersion-strengthened zirconium alloys. J. Less-Common Met. **8**, 36–46 (1965)
9. Z.N. Yang, F.C. Liu, F.C. Zhang, Z.G. Yan, Y.Y. Xiao, Microstructural evolution and mechanical properties in Zr705 during the rolling process. Mater. Sci. Eng. A **544**, 54–58 (2012)
10. L. Jiang, M.T. Perez-Prado, P.A. Gruber, E. Arzt, O.A. Ruano, M.E. Kassner, Texture, microstructure and mechanical properties of equiaxed ultrafine-grained Zr fabricated by accumulative roll bonding. Acta Mater. **56**, 1228–1242 (2008)
11. Z.N. Yang, F.C. Zhang, F.C. Liu, Z.G. Yan, Y.Y. Xiao, Achieving high strength and toughness in a Zr-2.3Nb alloy by the formation of duplex microstructure. Mater. Des. **40**, 400–406 (2012)
12. K. Lu, L. Lu, S. Suresh, Strengthening materials by engineering coherent internal boundaries at the nanoscale. Science **324**(5925), 349–352 (2009)
13. M. Wang, J.J. Beyerlein, J. Zhang, W.Z. Han, Defect-interface interactions in irradiated Cu/Ag nanocomposites. Acta Mater. **160**, 211–223 (2018)
14. J. Chen, L. Lu, K. Lu, Hardness and strain rate sensitivity of nanocrystalline Cu. Scr. Mater. **54**(11), 1913–1918 (2006)
15. D.J. Park, Y.I. Jung, J.H. Park, Y.H. Lee, H.G. Kim, Microstructural characterization of accident tolerant fuel cladding with Cr–Al alloy coating layer after oxidation at 1200 °C in a steam environment. Nucl. Eng. Technol. **52**(10), 2299–2305 (2020)
16. K. Lu, Stabilizing nanostructures in metals using grain and twin boundary architectures. Nat. Rev. Mater. **1**, 16019 (2016)
17. A. Sinha, S.K. Das, T.V. Vijaya, Synthesis of nanosized copper powder by an aqueous route. J. Mater. Synth. Process. **7**(6), 373–377 (1999)
18. O. Anderoglu, A. Misra, H. Wang, X. Zhang, Thermal stability of sputtered Cu films with nanoscale growth twins. J. Appl. Phys. **103**(9), 1357 (2008)
19. Y. Zhang, A. Godfrey, D.J. Jensen, Local boundary migration during recrystallization in pure aluminum. Scr. Mater. **64**(4), 331–334 (2011)
20. G.C. Hasson, C. Goux, Interfacial energies of tilt boundaries in aluminium: experimental and theoretical determination. Scr. Metal. **5**(10), 889–894 (1971)
21. A. Misra, R.G. Hoagland, H. Kung, Thermal stability of self-supported nanolayered Cu/Nb films. Philos. Mag. **84**(10), 1021–1028 (2004)
22. S. Zheng, I.J. Beyerlein, J.S. Carpenter, K.W. Kang, J. Wang, W.Z. Han, N.A. Mara, High-strength and thermally stable bulk

nanolayered composites due to twin-induced interfaces. Nat. Commun. **4**, 1696 (2013)

23. A. Misra, R.G. Hoagland, Effects of elevated temperature annealing on the structure and hardness of copper/niobium nanolayered films. J. Mater. Res. **20**, 2046–2054 (2005)
24. S. Cai, M.R. Daymond, R.A. Holt, Deformation of high β-phase fraction Zr-Nb alloys at room temperature. Acta Mater. **60**(8), 3355–3369 (2012)
25. M. Zhang, F.C. Zhang, Z.N. Yang, Y.N. Li, L. Qu, H.J. Zhen, Effect of cooling process on the formation of duplex microstructure in Zr-2.3Nb alloy. J. Alloys Compd. **651**, 316–321 (2015).
26. M. Zhang, Y.N. Li, F.C. Zhang, X.B. Wang, L.Y. Chen, Z.N. Yang, Effect of annealing treatment on the microstructure and mechanical properties of a duplex Zr-2.5Nb alloy. Mater. Sci. Eng. A **706**, 236–241 (2017).
27. Z.N. Yang, X.B. Wang, F. Liu, F.C. Zhang, L.J. Chai, R.S. Qiu, and L.Y. Chen: Effect of intercritical annealing temperature on microstructure and mechanical properties of duplex Zr-2.5Nb alloy. J. Alloys Compd. **776**, 242–249 (2019).
28. S. Banerjee, R. Tewari, P. Mukhopadhyay, Prog: Coupling of displacive and replacive ordering. Mater. Sci. **42**(1–4), 109–123 (1997)
29. J.C. Williams, D. De Fontaine, N.E. Paton, The ω-phase as an example of an unusual shear transformation. Metall. Trans. **4**(12), 2701–2708 (1973)
30. Y.F. Xu, D.Q. Yi, H.Q. Liu, B. Wang, F.L. Yang, Age-hardening behavior, microstructural evolution and grain growth kinetics of isothermal ω phase of Ti–Nb–Ta–Zr–Fe alloy for biomedical applications. Mater. Sci. Eng. A **529**, 326–334 (2011)
31. E.S.N. Lopes, A. Cremasco, C.R.M. Afonso, R. Caram, Effects of double aging heat treatment on the microstructure, Vickers hardness and elastic modulus of Ti–Nb alloys. Mater. Charact. **62**, 673–680 (2011)
32. B.S. Hickman, The formation of omega phase in titanium and zirconium alloys: a review. J. Mater. Sci. **4**, 554–563 (1969)
33. J. Smilauerova, P. Harcuba, J. Pospísil, Z. Matej, V. Holy, Growth of ω, inclusions in Ti alloys: an X-ray diffraction study. Acta Mater. **61**(17), 6635–6645 (2013)
34. S.M. Keralavarma, S. Chockalingam, A criterion for void coalescence in anisotropic ductile materials. Int. J. Plast. **82**, 159–176 (2016)
35. M.J. Nemcko, J. Li, D.S. Wilkinson, Effects of void band orientation and crystallographic anisotropy on void growth and coalescence. J. Mech. Phys. Solids **95**, 270–283 (2016)